Effect of pre-tensioning force on behavior of Buckling Restrained Brace (BRB) supported by double pre-tensioning system

Mohamed Selim, Muhammad E. Kamel, Eman Elshamy
Structural Engineering Dept., Faculty of Engineering, Zagazig University, Zagazig, 44519, Egypt
mselim940@gmail.com, https://orcid.org/0000-0002-5114-9644
muhammad.e.kamel@gmail.com, https://orcid.org/0009-0000-7142-1214
EAElshamy@ene.zu.edu.eg, https://orcid.org/0000-0001-9882-5905

Mohamed Emara
Structural Engineering Dept., Faculty of Engineering, Zagazig University, Zagazig, 44519, Egypt
Department of Civil Engineering, Delta Higher Institute for Engineering & Technology, Mansoura, Egypt
mremara@eng.zu.edu.eg, https://orcid.org/0000-0003-4936-5257

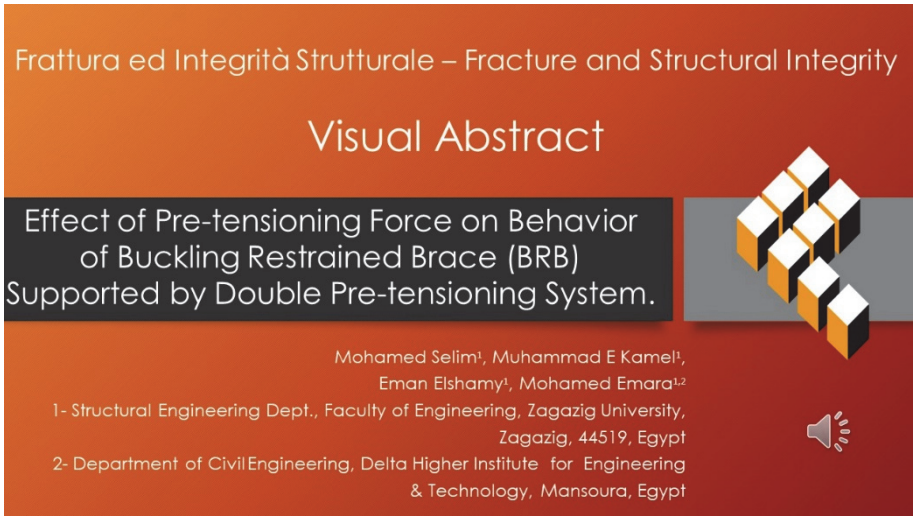

Citation: Mohamed Selim, Muhammad E. Kamel, Eman Elshamy, Mohamed Emara. Effect of pre-tensioning force on behavior of Buckling Restrained Brace (BRB) supported by double pre-tensioning system, Frattura ed Integrità Strutturale, 67 (2024) 205-216.

Received: 25.09.2023
Accepted: 03.12.2023
Online first: 05.12.2023
Published: 01.01.2024

KEYWORDS. All-steel BRBs, Pre-tensioning systems, Out-of-plane instability, Hysteretic behavior, Finite Element Analysis.

INTRODUCTION

Concentrically braced frames are commonly used as lateral resisting systems in steel structures. They provide high stiffness but have low ductility because of out-of-plane buckling [1, 2]. Energy-absorbing dampers can serve as effective damping systems [3-6]. By forming plastic hinges, these dampers prevent structural members from entering the nonlinear phase and buckling bracing members at intermediate seismic levels. This reduces the dynamic response of the structure to seismic loading [7-10].

The Buckling Restrained Brace (BRB) is a structural system designed to overcome limitations in moment-resisting frames (MRFs) and concentrically braced frames (CBFs) by providing sufficient stiffness and ductility. It consists of a central steel core enclosed in a buckling-restraint mechanism, which generates and dissipates energy through stable tension-compression hysteretic cycles, preventing brace buckling [11-13].

BRB development consists of three phases: The initial external restraining system comprises a concrete-infilled steel section combined with a steel core, which can take the form of a plate, I section, or other steel cross-section [14-17]. The complexities of pouring and curing concrete pose challenges in achieving precise configuration of the steel core and the gap between the concrete and steel core. All-steel BRB offers advantages such as easy on-site assembly, reduced weight, convenient replacement of inner core members, and inspection and reuse of external restraining systems [18, 19]. Researchers have further advanced the concept in earthquake engineering, developing various BRBs to maximize their potential in the field [19, 20].

Studies are ongoing to investigate the behavioral characteristics of BRBs, and there are advancements in the development of new devices [21-26]. In Japan, BRBs have been successfully tested for seismic protection of steel buildings, although their usage is currently limited. In this context, BRBs are considered as hysteretic dampers and are incorporated into moment-resisting frame MRFs that possess high stiffness and strength. Additionally, a dual system can be achieved by utilizing concentrically braced frames CBF with BRBs placed parallel to the MRF [27-29]. External restraining systems employ hollow cross-sections with either rectangular or circular shapes. To enhance the capacity of BRBs, it is necessary to increase the thickness of the element in relation to the inner core plate [30-33].

External restraining systems enable the inner core members to yield completely, leading to enhanced lateral stiffness and stable dissipation of hysteretic energy [34]. Buckling-restrained braces (BRBs) offer lateral stiffness and energy absorption during seismic events. They are commonly used in framed structures, long-span structures, and bridge structures to enhance the lateral resistance, energy dissipation capacity, and ductility [35, 36].

A new type of all-steel BRB, called pre-tensioned cable-stayed BRB (PCS-BRB), is proposed. This design adds a supplementary structural system of pre-tensioned cables and cross-arms on the exterior of a typical BRB. The external restraining system comprises of cable-stayed and outer restraining tubes, which enhance its external flexural stiffness. This design is suited for stadiums, high building, and other buildings where PCS-BRBs are exposed to high loads Guo et al [32, 37, 38].

Externally, pre-tensioned cable systems have been found to effectively increase the load-carrying capacity of slender compression members. This can be achieved by incorporating lateral cross-arms into the external casing discovered that a pre-tensioned system with a single cross-arm significantly enhances the member's overall capacity and improves the hysteretic response of BRB members. This method has demonstrated an improvement in the overall performance of BRBs [38].

This research aims to enhance rectangular BRBs with pre-tensioning systems. Finite Element Analysis (FEA) was used to investigate the impact of different configurations and initial pre-tensioning force values on traditional all-steel BRB members, in this study was performed through the following steps:

- Verification study on rectangular BRB using 3D finite Element Analysis.
- Using double pre-tensioning system on rectangular BRB to minimize thickness of external case.
- Parametric study on different parameters (pre-tensioning force value - steel grade).

NUMERICAL SIMULATION AND VERIFICATION

The main components of the studied BRB specimen are core plate, which represents the main item of the specimen, external case laterally supported by pre-tensioning steel cables to prevent the out-of-plane buckling. Two cross arms perpendicular to the external case were provided to connect the cables to the case. The steel core plate consists of a yielding segment, steel core projections, and transition segments. The axial friction between the core and the external case was avoided through a 2.5 mm gap between them. The FEA commercial code Abaqus 2020 [39] was used to simulate the behavior of the BRB. The eight-node solid element with linear reduced integration (C3D8R) was used to simulate the 3D model elements, including core, external case, and pre-tensioning cables, as shown in Fig. 1. The core plate lateral deformations put the core plate into contact with the external case, the surface-to-surface contact was utilized to simulate that contact. The contact properties used in normal and tangential directions were hard contact property and Coulomb-Mohr friction, respectively. The friction coefficient was 0.1. The Abaqus/Explicit analysis tool offers two approaches to constraint enforcement: "Hard" Contact, which uses the Lagrange multiplier technique, and "Penalty contact enforcement,"

which prevents surface separation after contact. A coupling constraint was used to prevent axial slipping of the external case.

The specimens were fixed from one end, allowing free axial movement at the other end at which the load was applied. The boundary conditions were applied to both ends through two reference points. The load was applied through two steps; the first steps included the application of the pre-tensioning force in cables, while a cyclic loading was utilized in the second step. A verification study on previous research was performed followed by a parametric study. A 50 mm mesh size was considered in the current study. The steel core plate and other model components were simulated using a bi-linear elastic-plastic stress-strain relationship, considering strain hardening effects as per AISC 358-16.

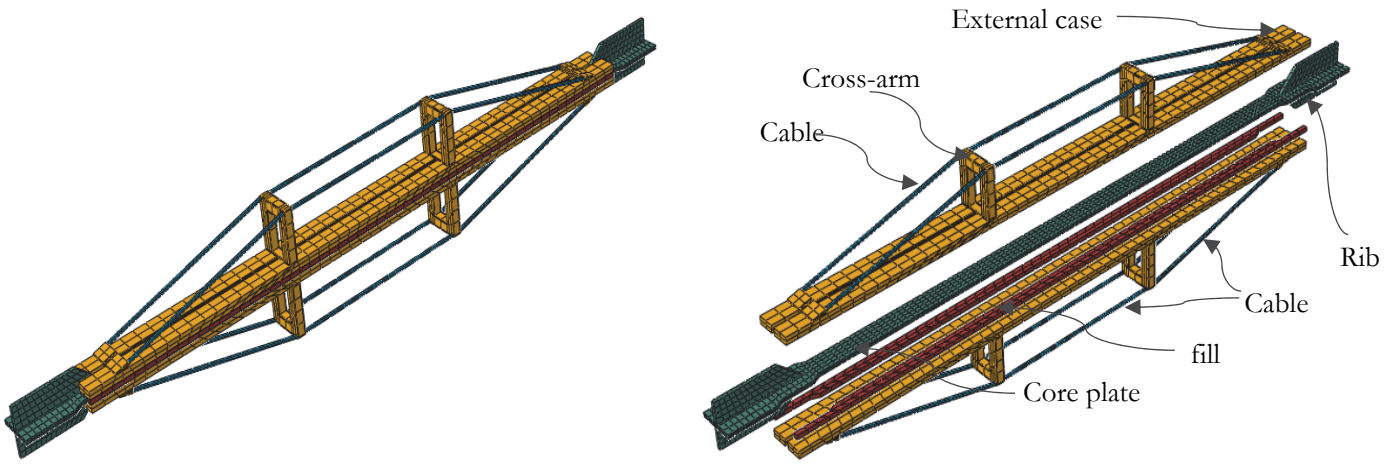

(a) Assembeled model **(b)** Model parts

Figure 1: BRB specimen details.

Verification

In this step, the model was verified against the experimental results of a BRB specimen tested by Wang et al [40]. where the tested specimen dimension (U-V1) is 1650 mm in total length, with a core plate yielding segment length (Ly) of 900 mm and width (w) of 10 mm as shown in Fig. 2

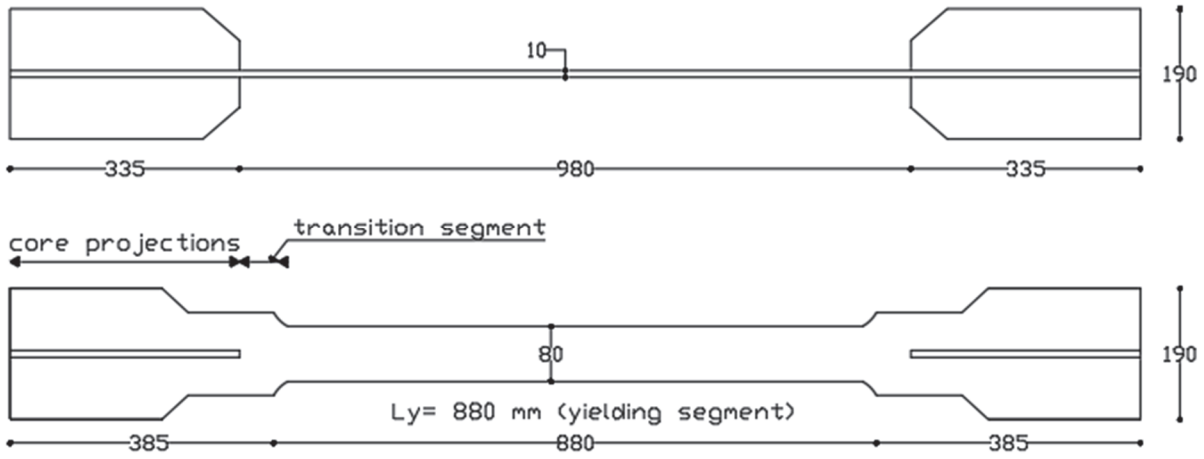

Figure 2: U-V1 specimen dimension.

The specimen underwent a cyclic load protocol. The initial axial stiffness in the elastic stage was measured using a strain amplitude of 0.75 ϵy . for the first four cycles. The subsequent loading phases consisted of variable strain amplitude (VSA) loading with increasing amplitudes, followed by constant strain amplitude (CSA) loading with a 2.0% amplitude. The

specimen U-V1 exhibited stable behavior before the 52nd loading cycle by constant strain amplitude CSA loading, respectively. FEA results presented an acceptable hysteretic behavior and good agreement with the experimental ones as shown in Fig. 3. Concerning failure mode, cracks in the transition segment near the rib were appeared in the FEA that were identical to the experimental results of Wang et al. [40] as shown in Fig. 4.

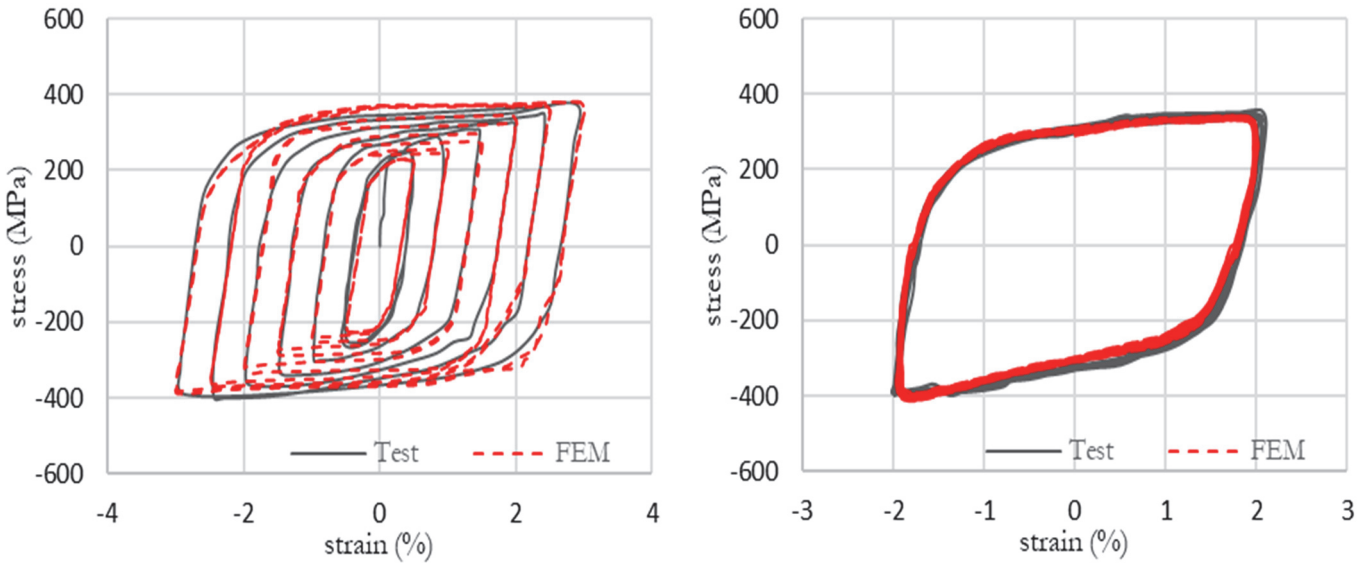

Figure 3: Experimental and FE hysteretic curve for specimen U-V1; (a) VSA phase, and (b) CSA phase.

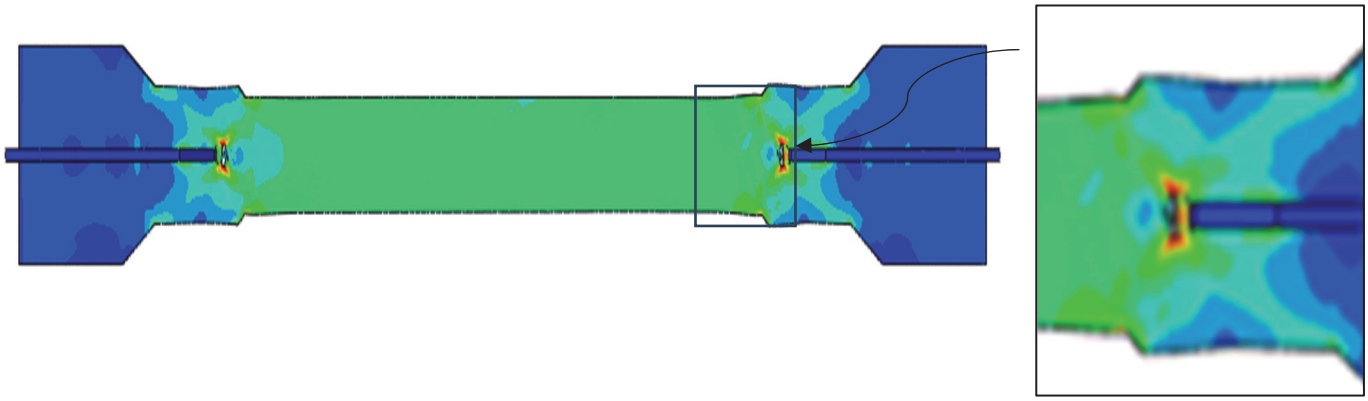

Figure 4: FE modes of failure specimen U-V1.

PARAMETRIC STUDY

This section inspected a five-story RC building with 6 m column spacing in both directions, X and Y, as shown in Fig. 5. The analysis and design were performed using the CSI ETABS program[41], according to ASCE [42] and ACI-318. The control BRB specimen was designed as a traditional all-steel member. A double-pre-tensioning system was provided to the external case, as shown in Fig. 1, in order to reduce the out-of-plane instability. The external case, provided with the pre-tensioning system, was redesigned to maintain the same load capacity, with a minimized thickness (Tc). The studied specimen's dimensions are presented in Fig. 6.

The study investigated the effect of different parameters on the behavior of 42 all-steel BRB models. The studied models were divided into four groups, as shown in Tab. 1. The initial pre-tensioning force was 40 kN, and different thicknesses were studied to achieve the same response as the traditional BRB control specimen in group G1. was applied to the double

pre-tensioning system. Groups G2, G3, and G4 were designed to study the effect of different material properties and a wide range of pre-tensioning forces (T0), as shown in Tab. 2.

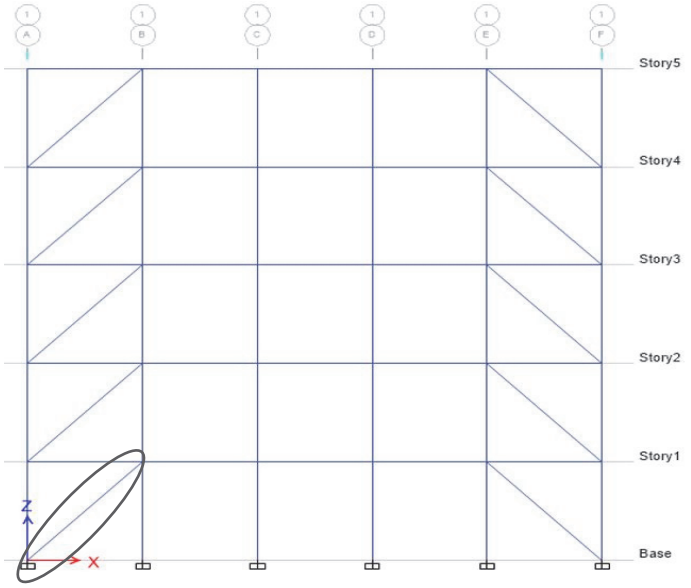

Figure 5: BRB location.

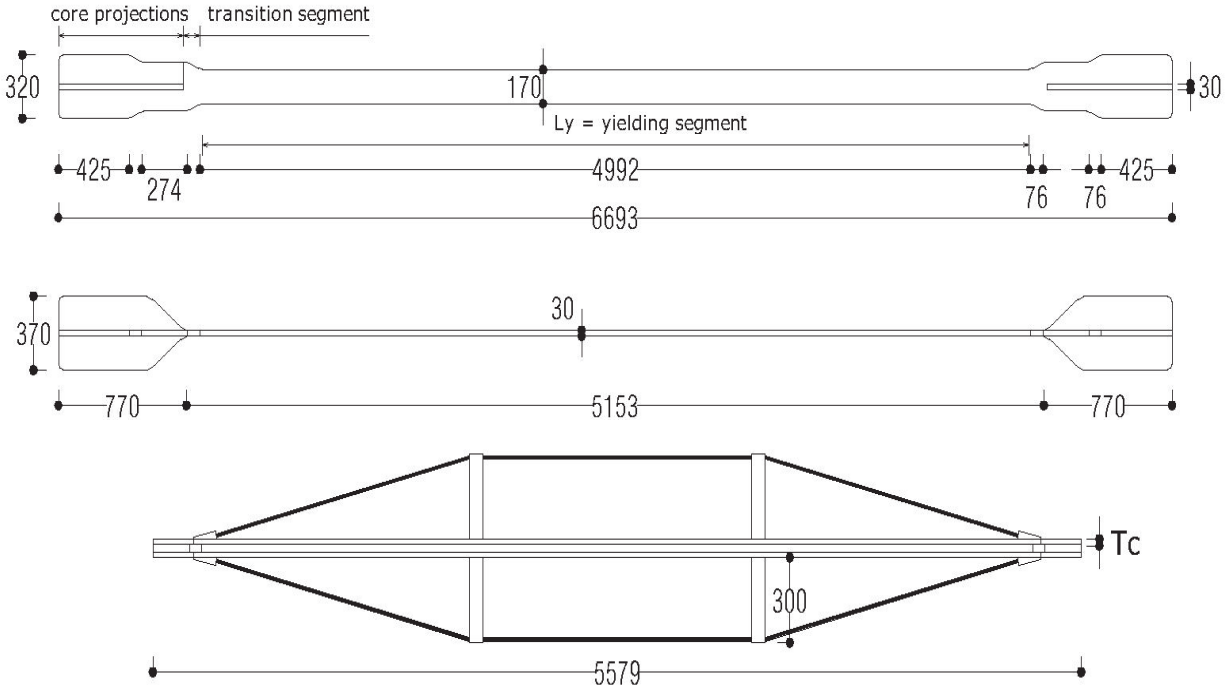

Figure 6: BRB specimen dimensions (Dimensions in mm).

Numerical simulation and loading

To consider the core plate imperfection and manufacturing defects, the first buckling mode was obtained through a nonlinear analysis. The specimens were subjected to cyclic loading with an incremental axial displacement at five levels. The applied displacements were ±5.70 mm (Δby) for the first two cycles, ±14.25 (0.5 Δbm) mm for the second two cycles, ±28.50 (1.0 Δbm) mm for the third two cycles, ±42.75 mm (1.5 Δbm) for the fourth two cycles, and ±57.00 mm (2.0 Δbm) for the fifth two cycles as shown in Fig. 7 [43]. Where Δby and Δbm represent the core plate yield displacement and brace axial deformation corresponding to the design story drift, respectively.

Group	Specimens ID	Core (b*t) mm	Loading	Pre-tensioning force (T0) kN	Steel
-	Control	30*175	Cyclic	-	St37
G1	P40-T50	30*175	Cyclic	40 kN	St 37
	P40-T40-St37			40 kN	
	P40-T30-St37			40 kN	
	P40-T25-St37			40 kN	
	P40-T20-St37			40 kN	
	P10-T20-St37			10 kN	
	P20-T20-St37			20 kN	
	P30-T20-St37			30 kN	
	P40-T20-St37			40 kN	
G2	P50-T20-St37	30*175	Monotonic	50 kN	St 37
	P60-T20-St37			60 kN	
	P70-T20-St37			70 kN	
	P80-T20-St37			80 kN	
	P90-T20-St37			90 kN	
	P100-T20-St37			100 kN	
	P110-T20-St37			110 kN	
	P120-T20-St37			120 kN	
G3	P10-T20-St44	30*175	Monotonic	10 kN	St 44
	P20-T20-St44			20 kN	
	P30-T20-St44			30 kN	
	P40-T20-St44			40 kN	
	P50-T20-St44			50 kN	
	P60-T20-St44			60 kN	
	P70-T20-St44			70 kN	
	P80-T20-St44			80 kN	
	P90-T20-St44			90 kN	
	P100-T20-St44			100 kN	
	P110-T20-St44			110 kN	
	P120-T20-St44			120 kN	
G4	P10-T20-St52	30*175	Monotonic	10 kN	St 52
	P20-T20-St52			20 kN	
	P30-T20-St52			30 kN	
	P40-T20-St52			40 kN	
	P50-T20-St52			50 kN	
	P60-T20-St52			60 kN	
	P70-T20-St52			70 kN	
	P80-T20-St52			80 kN	
	P90-T20-St52			90 kN	
	P100-T20-St52			100 kN	
	P110-T20-St52			110 kN	
	P120-T20-St52			120 kN	

Table 1: Studied BRB groups.

Steel type	E(MPa)	σ_y (MPa)	ε_y (%)	σ_u (MPa)	ε_u (%)
St 37	205	235	.33	353	25.1
St 44	205	274	.34	431	23.2
St 52	205	353	.36	509	22.2

Table 2: Material properties (E: Modulus of elasticity, σ_y: yield strength, ε_y: yield strain, σ_u: ultimate strength, ε_u: ultimate strain,)

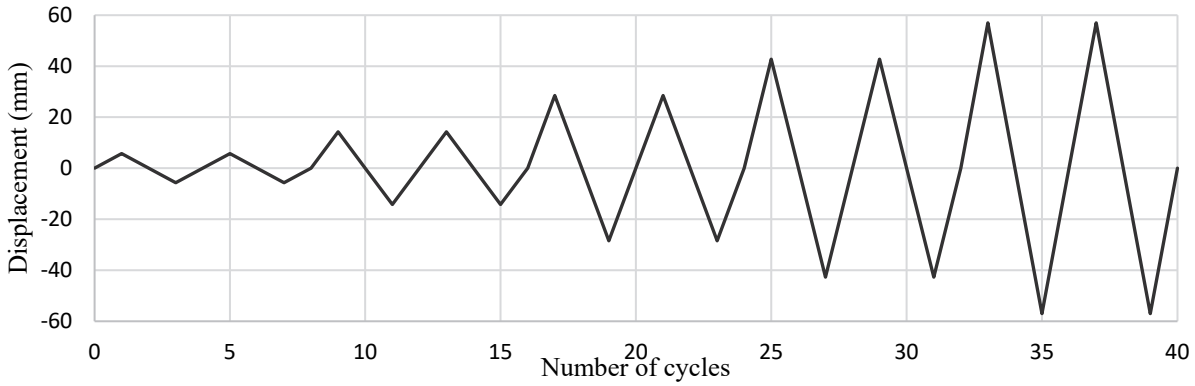

Figure 7: Loading protocol [43].

The minimum thickness for the double pre-tensioning system

A parametric study was conducted to find the minimum thickness for the external case of the double pre-tensioning stem. T study compared the compression stage of the backbone curve, as shown in Fig. 8, the deformed shape along the core plate length, and overall hysteretic load-displacement curves. The results showed that providing the double pre-tensioning system to specimens of P40-T50-St37 mm and P40-T40-St37 mm thickness achieved higher capacities and balanced hysteretic behavior. However, decreasing the external case thickness from P40-T30-St37 mm to P40-T15-St37 mm led to degradation in axial stiffness and a deformed core plate shape, as shown in Fig. 9. The P40-T20-St37 mm thickness was considered as the minimum thickness for the external case of the double-pre tensioned model, saving about 66% of the outer case thickness compared to the control BRB.

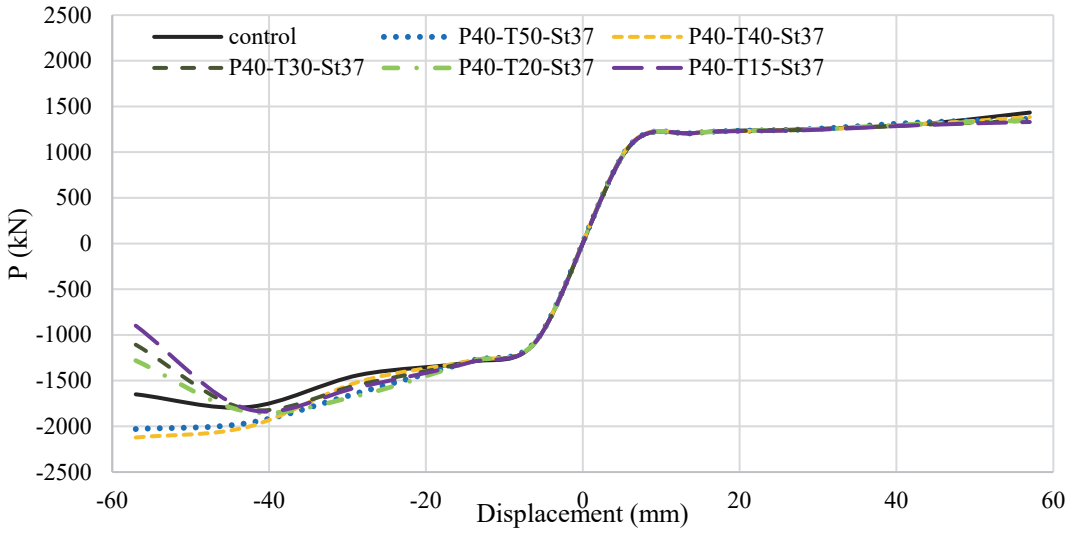

Figure 8: Double arm minimizes thickness compression stage backbone curve.

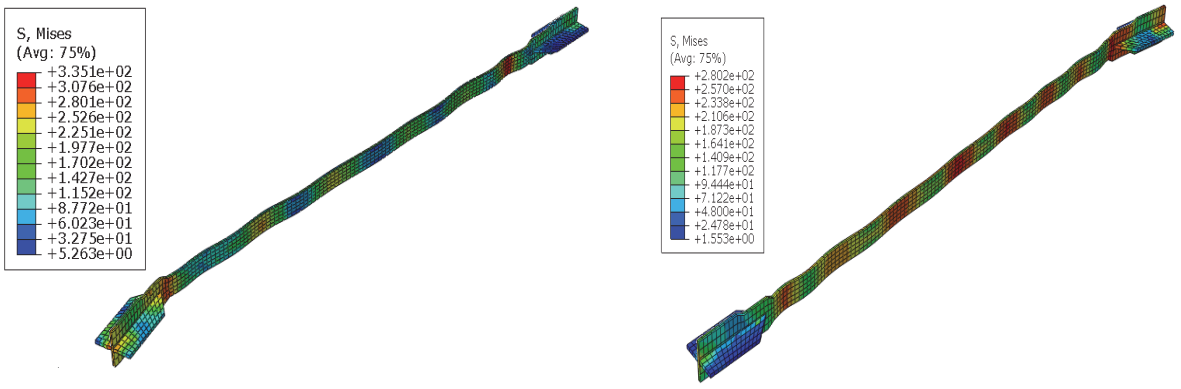

(a) (b)

Figure 9: Deformed shape and stresses for double arm minimize thickness (a) St37-P40-II-T15, and (b) St37-P40-II-T20.

EFFECT OF INITIAL PRE-TENSIONING FORCE

This section studied the effect of the initial pre-tensioning force value, where the pre-tensioning force is first applied uniformly to all cables using stress es. ABAQUS then iteratively adjusts the stress difference among the cables until the desired pre-tensioning force is attained. A wide range from 10 to 120 kN was assigned to the initial pre-tensioning force. The BRBs capacity (P) were obtained and compared to that of the control BRB (P0). Fig. 10 shows that increasing the initial pre-tensioning force increased the member load capacity with an ascending rate up to 70 kN, 50 kN, and 40 kN for steel St37, St44, and St52, respectively. As shown in Fig. 10, the specimens were divided into four sub-ranges based on the pre-tensioning force value: 10-30 kN (Range I), 40-60 kN (Range II), 70-80 kN (Range III), and 90-120 kN (Range IV).

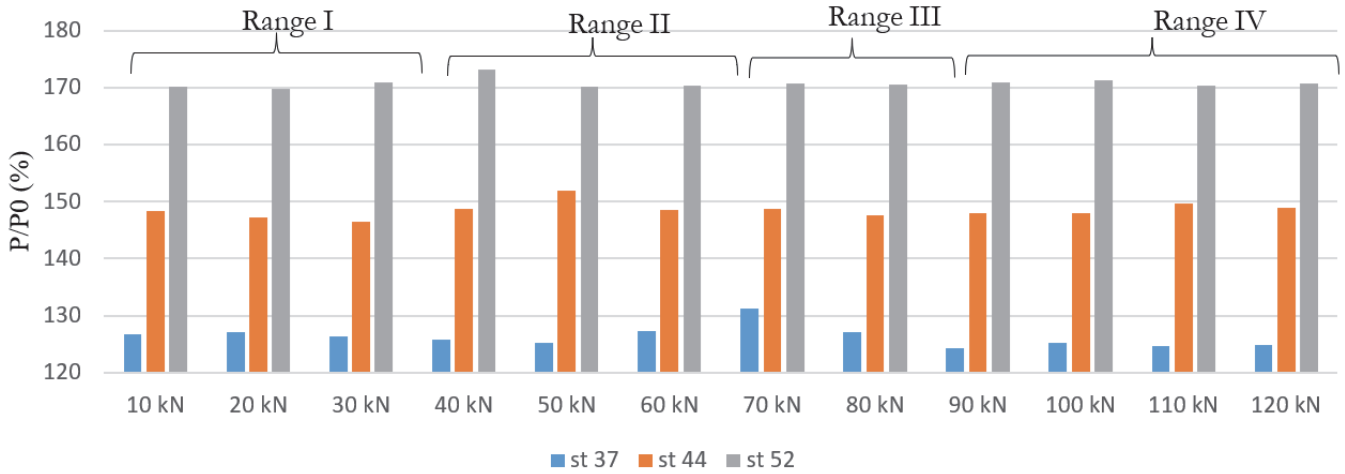

Figure 10: Effect of initial pre-tensioning force range.

EFFECT OF STEEL TYPE

In this section, the impact of steel type on the performance of all steel BRB with a double pre-tensioning system is examined. The variation in pre-tensioning force (ΔT) concerning the axial deformation of the core is illustrated in Figs. 11 to 13, considering different initial pre-tensioning forces. The variation in pre-tensioning force was determined as the difference between the actual pre-tensioning force value (T) and the initial pre-tensioning force value (T0) where the pre-tensioning force value (T) was extracted from the middle point of the cable.

Steel 37

In Range I (from 10 kN to 30 kN), insignificant additional pre-tensioning forces appeared in cables for 20 kN and 30 kN.

On the other hand, after reaching a displacement of 90 mm, an additional pre-tensioning force was registered except for the case of 10 kN, as illustrated in Figs. 11(a). Moreover, increasing the initial pre-tensioning force had no effect on the overall behavior of the BRB specimen as a result of necking phenomena that was noticed in the inner core accompanied with local buckling at low loading range.

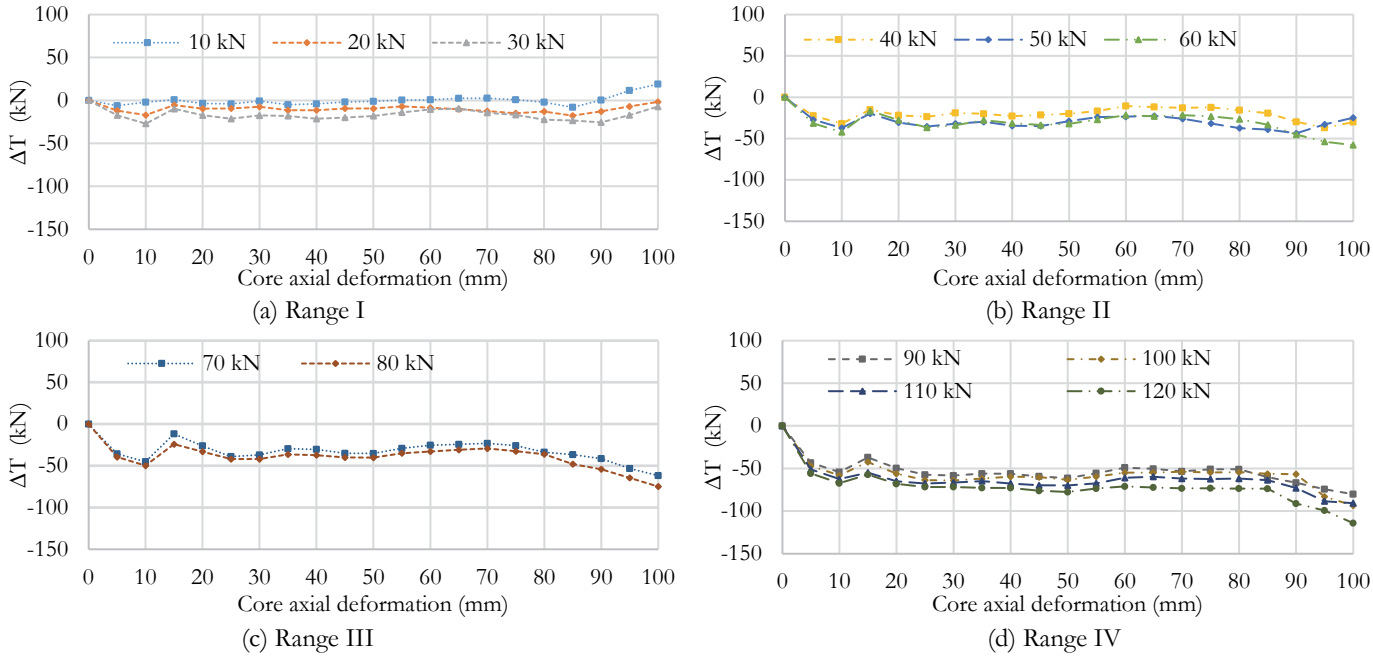

(a) Range I (b) Range II

(c) Range III (d) Range IV

Figure 11: Difference in cable pretension force for all ranges for steel 37.

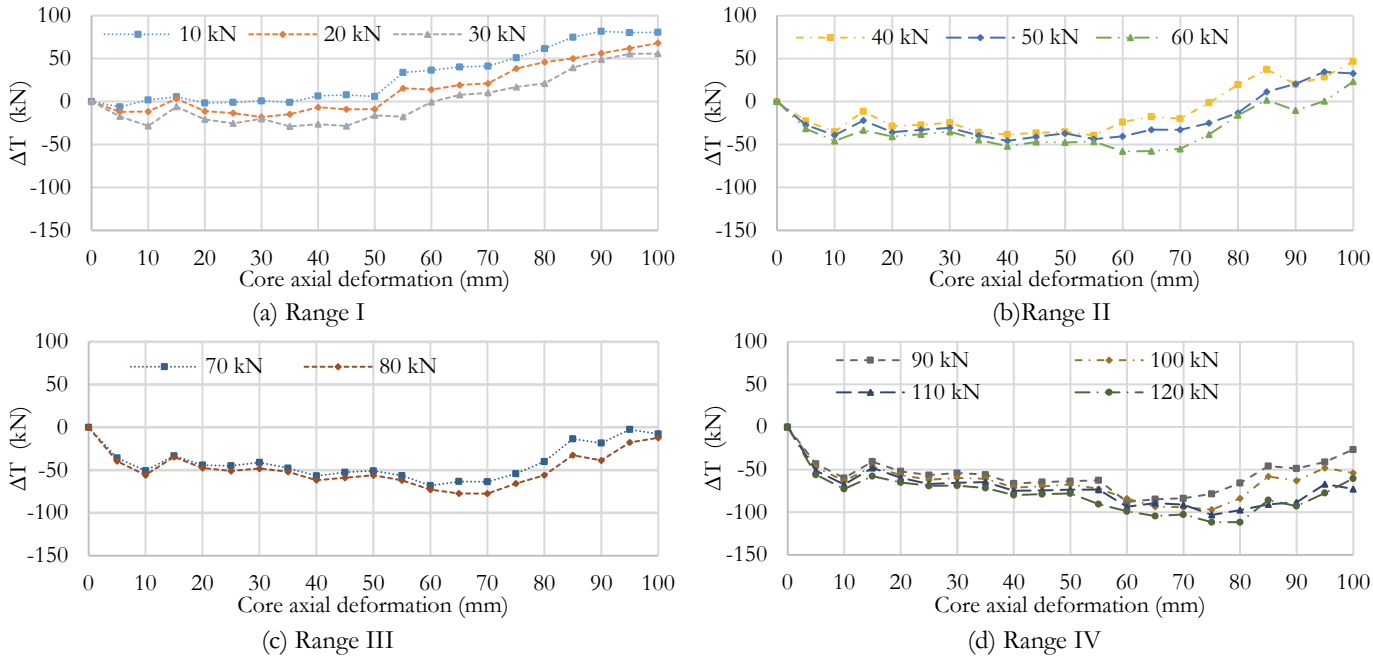

(a) Range I (b)Range II

(c) Range III (d) Range IV

Figure 12: Difference in cable pretension force for all ranges for steel 44.

Steel 44

For steel 44, an additional pre-tensioning force occurred in case of both range I and II. The force started to appear when the core axial deformation reached 50-60 mm and 75-85 mm for range I and II, respectively as shown in Fig. 12 (a) and (b). For both ranges III and IV, no additional pre-tensioning force was observed in cables up to failure. Moreover, the necking

phenomena occurred at loading range higher than that of steel 37.

Steel 52

Using steel 52 enhanced the contribution of the pre-tensioning cables as an additional pre-tensioning force appeared in the first three ranges (I, II, and III) as shown in Fig. 13 (a). In range I, the cables exerted additional forces at core axial deformation of about 25-35 mm. while, in case of range II and III, the additional force appeared at core axial deformation of about 40-60 mm and 65-70 mm, respectively. On the other hand, no additional pre-tensioning force was observed in the last range (range IV).

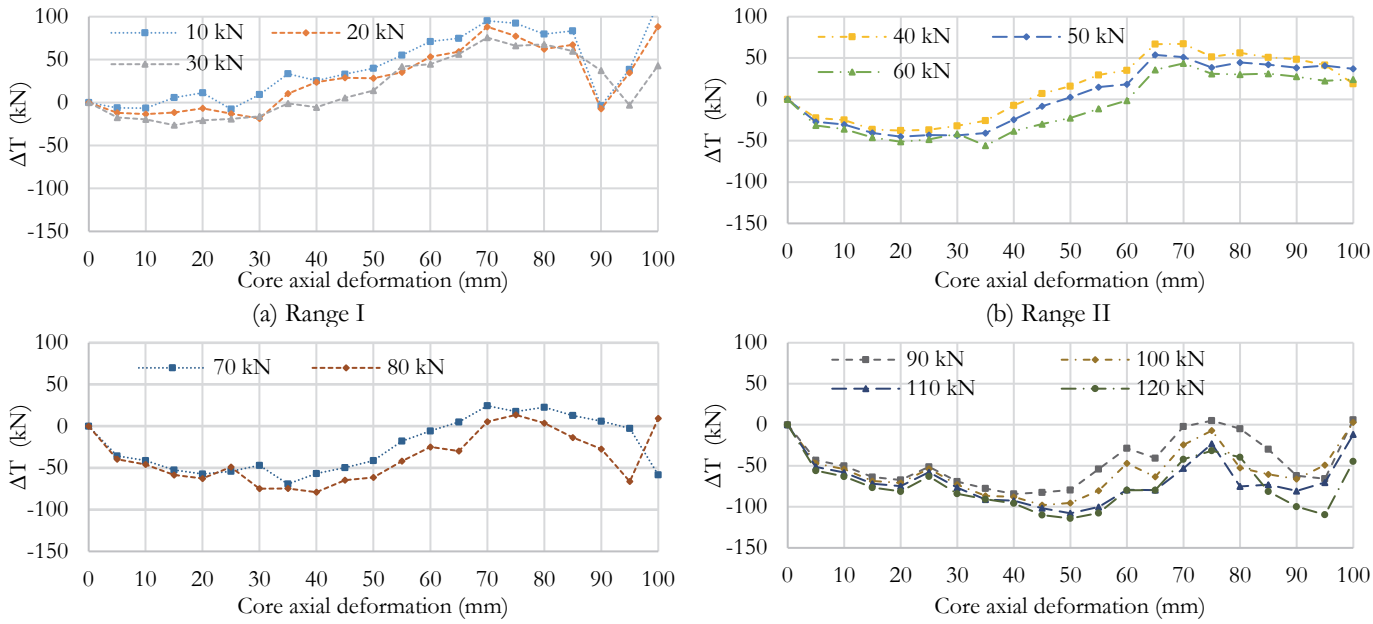

Figure 13: Difference in cable pretension force for all ranges for steel 52.

Conclusions

This paper presented a study of the effect of the pre-tensioning forces system on the behavior of an all-steel buckling restrained brace (BRB) using a numerical analysis program (ABAQUS). This study aimed to investigate the effectiveness of adding a double pre-tensioning system to traditional BRB members to reduce thickness. The main parameters studied were the initial pre-tensioning force value in the cables and its impact on member capacity, as well as the effect of steel used, where used three types of steel with different grades as the strength of the element increases as the steel grade. During this study, these outcomes were achieved.

- The axial compressive load-carrying capacity of traditional buckling restrained brace can be effectively enhanced by applying the proposed pre-tensioning system.
- The specimens with additional double pre-tensioning system with force in cable 70 kN, 50 kN, and 40 kN provided the capacity of BRB member by 31%, 51%, and 73.2 % for steel 37, 44, and 52, respectively, over than the capacity of design specimen without a pre-tensioning system.
- With the addition of the double pre-tensioning system on BRB member, it reduces the thickness of the external member by 66% (from 60 mm to 20 mm).
- The application of the pre-tensioning system increased the axial capacity of all studied BRB specimens.
- Increasing the pre-tensioning force value increased the BRB capacity up to 10 kN, 60 kN, and 80 kN for steel 37, 44, and 52, respectively.

REFERENCE

[1] Zhang, W., Xie, J., Liu, Y. and Ding, Y., (2023).Experimental investigation on steel bracing members with bolted gusset plate connections. Journal of Building Engineering. 107133.

[2] Almohammad-Albakkar, M. and Behnamfar, F., (2022).Numerical investigation of grooved gusset plate damper for using in cross-braced frames. Journal of Constructional Steel Research. 196, 107434.

[3] Zhu, Y., Wang, W., Lu, Y. and Yao, Z., (2023).Finite element modeling and design recommendations for low-yield-point steel shear panel dampers. Journal of Building Engineering. 72, 106634.

[4] Moghaddam, S. H. and Shooshtari, A., (2023).Numerical and experimental investigation on seismic performance of proposed steel slit dampers. Journal of Constructional Steel Research. 200, 107646.

[5] Chen, Z., Dai, Z., Huang, Y. and Bian, G., (2013).Numerical simulation of large deformation in shear panel dampers using smoothed particle hydrodynamics. Engineering structures. 48, pp. 245-254.

[6] Shobeyri, G., (2023).Improved MPS gradient models for elasticity problems. Iranian Journal of Science and Technology, Transactions of Civil Engineering. 47(3), pp. 1831-1843.

[7] Qu, B., Dai, C., Qiu, J., Hou, H. and Qiu, C., (2019).Testing of seismic dampers with replaceable U-shaped steel plates. Engineering Structures. 179, pp. 625-639.

[8] Chen, S., Wang, W., Zhou, C., Huang, Z. and Hua, X., (2023).Damping Capacity and Seismic Performance of a Torsional Metallic Damper Using a Displacement Amplification Mechanism. Journal of Bridge Engineering. 28(10), 04023071.

[9] Xiang, Y., Zhou, X., Ke, K., Shi, Y. and Xu, L., (2023).Experimental research on seismic performance of cold-formed thin-walled steel frames with braced shear panel. Thin-Walled Structures. 182, 110210.

[10] Pan, X. and Yang, T., (2023).3D vision-based out-of-plane displacement quantification for steel plate structures using structure-from-motion, deep learning, and point-cloud processing. Computer-Aided Civil and Infrastructure Engineering. 38(5), pp. 547-561.

[11] Chou, C.-C., Tsai, W.-J. and Chung, P.-T., (2016).Development and validation tests of a dual-core self-centering sandwiched buckling-restrained brace (SC-SBRB) for seismic resistance. Engineering Structures. 121, pp. 30-41.

[12] Zhou, Z., He, X., Wu, J., Wang, C. and Meng, S., (2014).Development of a novel self-centering buckling-restrained brace with BFRP composite tendons. Steel and composite structures. 16(5), pp. 491-506.

[13] Wang, C., Li, T., Chen, Q., Wu, J. and Ge, H., (2014).Experimental and theoretical studies on plastic torsional buckling of steel buckling-restrained braces. Advances in Structural Engineering. 17(6), pp. 871-880.

[14] Zhou, Y., Zhang, Q., Zhou, Y., Zhang, Y., Li, M., Feng, J. and Cai, J., (2023).Buckling-controlled braces for seismic resistance inspired by origami patterns. Engineering Structures. 294, 116771.

[15] Benavent-Climent, A., González-Sanz, G., Donaire-Avila, J., Galé-Lamuela, D. and Escolano-Margarit, D., (2023). Seismic response of a rc structure with new self-centering metallic dampers under biaxial near-field ground motions: shake table tests. Journal of Building Engineering. 65, 105753.

[16] Ghandil, M., Riahi, H. T. and Behnamfar, F., (2023).Numerical and experimental studies on a new metallic-yielding pistonic damper based on pure-bending flexural yielding mechanism. Journal of Building Engineering. 107690.

[17] Yan, X., Alam, M. S., Shu, G. and Qin, Y., (2023).A novel self-centering viscous damper for improving seismic resilience: Its development, experimentation, and system response. Engineering Structures. 279, 115632.

[18] Zhang, C., Zong, S., Sui, Z. and Guo, X., (2023).Seismic performance of steel braced frames with innovative assembled self-centering buckling restrained braces with variable post-yield stiffness. Journal of Building Engineering. 64, 105667.

[19] Lu, Y., Liu, Y., Wang, Y., Liu, J. and Huang, X., (2023).Development of a novel buckling-restrained damper with additional friction energy dissipation: Component tests and structural verification. Engineering Structures. 274, 115188.

[20] Kazemi, F. and Jankowski, R., (2023).Seismic performance evaluation of steel buckling-restrained braced frames including SMA materials. Journal of Constructional Steel Research. 201, 107750.

[21] Bregoli, G., Genna, F. and Metelli, G., (2016).Analytical estimates for the lateral thrust in bolted steel buckling-restrained braces. Journal of Mechanics of Materials and Structures. 11(2), pp. 173-196.

[22] Zhong, Y.-L., Li, G.-Q., Xiang, Y. and Wang, Y.-Z., (2023).Ultra-low cycle fatigue life prediction of assembled steel rod energy dissipaters with calibrated ductile fracture models. Engineering Structures. 285, 116002.

[23] Vazquez-Colunga, S. Y., Lee, C. L. and MacRae, G. A., (2018).Effects of out-of-plane displacements on load capacity of gusset plates in buckling restrained braced frames. Key Engineering Materials. 763, 892-899.

[24] Deng, K., Pan, P., Nie, X., Xu, X., Feng, P. and Ye, L., (2015).Study of GFRP steel buckling restraint braces. Journal of Composites for Construction. 19(6), 04015009.
[25] Deng, K., Pan, P., Li, W. and Xue, Y., (2015).Development of a buckling restrained shear panel damper. Journal of Constructional Steel Research. 106, pp. 311-321.
[26] Dehghani, M. and Tremblay, R., (2018).Design and full-scale experimental evaluation of a seismically endurant steel buckling-restrained brace system. Earthquake Engineering & Structural Dynamics. 47(1), pp. 105-129.
[27] Suzuki, A. and Kimura, Y., (2023).Rotation capacity of I-shaped beam failed by local buckling in buckling-restrained braced frames with rigid beam-column connections. Journal of Structural Engineering. 149(2), 04022243.
[28] Karami, M., Estekanchi, H. E., Hajirasouliha, I. and Mirfarhadi, S. A., (2023).Optimal Properties of Nonlinear Viscous Dampers in Steel Structures Considering the Life Cycle Cost. Journal of Earthquake Engineering. pp. 1-24.
[29] Zhou, X., Tan, Y., Ke, K., Yam, M. C., Zhang, H. and Xu, J., (2023).An experimental and numerical study of brace-type long double C-section steel slit dampers. Journal of Building Engineering. 64, 105555.
[30] Zhu, B.-L., Guo, Y.-L., Gao, J.-K. and Pi, Y.-L., (2020).Behaviour and design of spatial triple-truss-confined BRBs with a longitudinal shuttle shape. Engineering Structures. 215. DOI: 10.1016/j.engstruct.2020.110605.
[31] Heidary-Torkamani, H. and Maalek, S., (2017).Conceptual numerical investigation of all-steel Tube-in-Tube buckling restrained braces. Journal of Constructional Steel Research. 139, pp. 220-235.
[32] Guo, Y.-L., Fu, P.-P., Zhou, P. and Tong, J.-Z., (2016).Elastic buckling and load resistance of a single cross-arm pre-tensioned cable stayed buckling-restrained brace. Engineering Structures. 126, pp. 516-530.
[33] Guo, Y.-L., Zhu, J.-S., Zhou, P. and Zhu, B.-L., (2017).A new shuttle-shaped buckling-restrained brace. Theoretical study on buckling behavior and load resistance. Engineering Structures. 147, pp. 223-241.
[34] Watanabe, A., Hitomi, Y., Saeki, E., Wada, A. and Fujimoto, M. (1988). Properties of brace encased in buckling-restraining concrete and steel tube. in Proceedings of ninth world conference on earthquake engineering.
[35] Sutcu, F., Takeuchi, T. and Matsui, R., (2014).Seismic retrofit design method for RC buildings using buckling-restrained braces and steel frames. Journal of Constructional Steel Research. 101, pp. 304-313.
[36] Bazaez, R. and Dusicka, P. (2015). Design implementation of buckling restrained braces for seismic retrofitting of reinforced concrete multi-column bridge bents. in Structures Congress 2015.
[37] Guo, Y.-L., Zhou, P., Fu, P.-P., Zhu, B.-L. and Wang, M.-Z., (2019).Experimental test and hysteretic behavior of single cross-arm PCS-BRBs. Journal of Constructional Steel Research. 160, pp. 223-239. DOI: 10.1016/j.jcsr.2019.05.036.
[38] Zhou, P., Zhu, B.-L., Guo, Y.-L. and Li, J.-Y., (2020). Performance and design of double cross-arm cable-stayed buckling-restrained braces with fix-ended stays. Journal of Constructional Steel Research. 173, pp. 106238.
[39] 3DS. (2020). Abaqus 2020 Products.
[40] Chen, Q., Wang, C.-L., Meng, S. and Zeng, B., (2016). Effect of the unbonding materials on the mechanic behavior of all-steel buckling-restrained braces. Engineering Structures. 111, pp. 478-493.
[41] ETABS. csi: www.csiamerica.com.
[42] Bernuzzi, C. and Cordova, B., (2016). Structural steel design to Eurocode 3 and AISC specifications. John Wiley & Sons.
[43] Safety, I. S., (2003). Recommended Provisions for Seismic Regulations for New Buildings and Other Structures (FEMA 450). FEMA: Washington, DC, USA.